Neutron track length estimator for GATE Monte Carlo dose calculation in radiotherapy

H. Elazhar, T. Deschler, Jean Michel Létang, A. Nourreddine, N. Arbor

Physics in Medicine and Biology

Neutron track length estimator for GATE Monte Carlo dose calculation in radiotherapy

To cite this article before publication: Halima Elazhar *et al* 2018 *Phys. Med. Biol.* in press https://doi.org/10.1088/1361-6560/aac768

Neutron track length estimator for GATE Monte Carlo dose calculation in radiotherapy

H. Elazhar[1*], T. Deschler[1], J.M Létang[2], A. Nourreddine[1], N. Arbor[1]

1. Institut Pluridisciplinaire Hubert Curien (IPHC), Université de Strasbourg
23 rue du Loess, 67037 Strasbourg Cedex, France

2. Univ Lyon, INSA-Lyon, Université Claude Bernard Lyon 1, UJM-Saint Etienne, CNRS, Inserm
Centre Léon Bérard, CREATIS UMR 5220, U1206, F-69373, Lyon, France

* Corresponding author : halima.elazhar@iphc.cnrs.fr

Abstract

The out-of-field dose in radiation therapy is a growing concern in regards to the late side-effects and secondary cancer induction. In high-energy X-ray therapy, the secondary neutrons generated through photonuclear reactions in the accelerator are part of this secondary dose. The neutron dose is currently not estimated by the treatment planning system (TPS) while it appears to be preponderant for distances greater than 50 cm from the isocenter. Monte Carlo (MC) simulation has become the gold standard for accurately calculating the neutron dose under specific treatment conditions but the method is also known for having a slow statistical convergence, which makes it difficult to be used on a clinical basis. The nTLE (neutron TLE), a neutron variance reduction technique inspired by the track length estimator (TLE) method has thus been developped for the first time in the Monte Carlo code GATE to allow a fast computation of the neutron dose in radiotherapy. The details of its implementation, as well as the comparison of its performances against the analog MC method, are presented here. A gain of time from 15 to 400 can be obtained by our method, with a mean difference in the dose calculation of about 1% in comparison with the analog MC method.

Keywords : Track length estimator, GATE, Monte Carlo simulation, Neutron dose calculation, Radiotherapy

1 Introduction

Modern radiotherapy techniques based on the use of a linear accelerator aim to achieve better control for deep-seated tumours. However, they also can be responsible for the development of late side-effects and secondary cancers which today is a debated topic among scientific and medical groups.The literature reports mainly information on the organs at risk located next to the target volume (Xu et al. 2008, Takam et al. 2011). These organs are usually irradiated with high doses: this leads to a high probability of normal tissue complications and usually to a small risk of radiation-induced second primary cancer (Takam et al. 2011). During a radiotherapy treatment, besides its therapeutic dose, the patient gets exposed to sources of secondary dose which include the photon secondary dose. Indeed, the use in X-ray therapy of electron accelerators contributes to the out-of-field doses to patient by leakage and scattering of the primary photon beam (Halg et al. 2012). This photon secondary dose can vary considerably depending on the photon energy, treatment modality, irradiation

geometry, size of the tumour and patient, as well as the distance from the irradiated volume: a typical secondary dose is some hundreds of mSv 10 cm away from the target volume ((Gudowska et al. 2014)) over the course of a treatment. Adding to that, modern linear accelerators are usually equipped with on-board imaging (OBI) devices, allowing 3D on-line patients set-up and verification by using cone beam computed tomography (CBCT) (Palm et al. 2010). The additional radiation doses from CBCT can significantly increase out-of-field doses to patients in case of frequent patient set-up during the radiotherapy treatment. Depending on the CBCT type, the mean delivered dose can range from 3 mGy to 100 mGy (Palm et al. 2010). Besides this photon dose, for accelerators operating at energies above photonuclear reactions thresholds (1.66 MeV (Be), 6.5 MeV (W), 10 MeV (Cu)), neutrons produced through (γ,n) reactions in the bremsstrahlung target, flattening filter, collimators, shielding materials inside the treatment head and inside the patient's body are another source of unwanted doses delivered to the patient (D'Errico et al. 1998, Akkurt et al. 2003, Naseri et al. 2010). The patient entire body will be exposed to this out-of-field radiation. Several dosimetry studies have been carried out through measurement and modelling techniques and have shown the relationship existing between out-of-field dose and radiation induced secondary cancer (Brenner et al. 2000, Newhauser et al. 2011, Murray et al. 2014). However, through these studies, a whole range of equivalent doses (and thus associated risks) has been reported leading to the need for additional studies for these dosimetric concerns. In the literature, regardless of the measurement technique and type of accelerator, the neutron dose equivalent per unit photon dose can range from as low as 0.1 mSv/Gy to as high as 20.4 mSv/Gy (Takam et al. 2011).

Moreover, it has been reported that at some specific locations the neutron dose becomes larger than the photon dose, leading to a larger neutron-to-photon absorbed dose ratio (Carinou et al. 2005). This neutron production, which is related to the patient irradiation configuration, has been shown to be more important for IMRT (Intensity Modulated Radiotherapy) treatment than for 3D-CRT (3D-Conformal Radiotherapy)(Howell et al. 2006, Reft et al. 2006). In regards to their high relative biological effectiveness reflected in their high radiation weighting factors (ICRP 2007), it is important to estimate their related dose, especially when we know that neutron spectra produced by medical linear accelerators have mean energies between 0.5 and 1 MeV that correspond to the highest radiation weighting factors. So far, no current treatment planning system (TPS) is computing this neutron dose.

Radiation doses from neutrons can be calculated by the use of a Monte Carlo simulation code such as MCNP (Shultis et al. 2006, Carinou et al. 2005, Mesbahi et al. 2009), FLUKA (Ferrari et al. 2005, Huang et al. 2005, Chen et al. 2006) and Geant4 (Jarlskog et al. 2008, Athar et al. 2010). The results obtained by simulation can have a high degree of precision depending on the accuracy of the data (i.e nuclear cross sections) and parameters. However, they can be difficult to use on a clinical basis because a long calculation time is required, particularly if low threshold (cut-off) energies of modeled particles are used. That is why, there is a real need for developing a tool that will allow a decrease in the neutron simulation time to make neutron dose calculation more accessible on a clinical basis.

The most commonly used standard variance reduction techniques (VRT) such as the absorption supression, splitting and Russian roulette, forced collision, and source biasing have mainly been developped for photon dosimetry (Seco & Verhaegen 2013). In MCNP, the comparison of two VRT used for neutron transportation,

the APDT (Adjoint Point Detector Technique known as the DXTRAN technique) and the LEXT (Legendre EXpansion Technique) have showed that the latter is 6 to 20 times faster than the analog MC (Nievaart et al. 2007). In FLUKA, the non-analog neutron absorption technique (also known as survival biasing) and the biased down scattering are also used as VRT techniques. Through all the VRT, the track length estimator (TLE) method is known as an efficient tallying method, suitable for kerma calculations at any given point in photons irradiations cases (Williamson 1987). It has been used for a long time (Williamson 1987, Carlsson 1985) and is implemented in different codes such as MCNPX (DeMarco et al. 2002, Smans et al. 2010) and in some specific tools for external radiotherapy (Van der Zee et al. 2005) and brachytherapy (Chibani et al. 2005, Taylor et al. 2007).

Many Monte Carlo simulation tools have been developed for dosimetry purposes (Pelowitz 2008, Battistoni et al. 2007, Ferrari et al. 2005, Perl et al. 2012, Walters et al. 2002, Kawrakow et al. 2000). GATE (Jan et al. 2004) constitute an open-source MC simulation platform that can support a user-friendly simulation framework of imaging (Jan et al. 2011) and dosimetry (Sarrut et al. 2014) in a same environment. This software is based on the GEANT4 toolkit. GATE is also used in radiotherapy applications for comparisons with MC TPS (Luceski et al. 2013). With the GATE V6.2 release, a specific VRT option based on the track length estimator (TLE) has been implemented for low-energy photon dose calculation (Mittone et al. 2013). This method allows an efficiency gain between 10 and 10^3 depending on the simulation set-up. In the latest release (GATE V7.2), two extra low energy photon VRT, namely force detection (Poludniowski et al. 2009) and exponential TLE (Smekens et al. 2009, Smekens et al. 2014) have been developed. However, no current version of GATE does currently include a VRT for neutron dose calculation.

In such a context, it seemed interesting to develop a tool that will allow a precise calculation of the secondary neutron dose in RT in a shorter time than the analog Monte Carlo simulation. To do so, the treatment planning parameters (field size, beam energy, angulation...) can be retrieved through the generated DICOM files (RTplan). This information would be retrospectively reprocessed after each treatment to be used as an input for MC calculations of 3D neutrons (and photons) dose maps.

While many VRT are available in MC TPS and used in clinical routine for photon dose calculation, the objective of our work was to add a neutron VRT in the GATE framework in order to set up a tool that would generate neutron dose maps (to be systematically recorded during the treatment). In such a way, we aim to achieve the generation of a dosimetric database on out-of-field dose that can be used for future epidemiological studies in order to improve low dose-risk models.

1.1 Method

1.1.1 TLE method in GATE for photons

The TLE method has been implemented in GATE for low energy X-rays (Mittone et al. 2013) and prompt γ (Huisman et al. 2016). It allows to calculate the particle fluences, kerma and absorbed dose.

In charged particle equilibrium (CPE), for a monoenergetic photon beam the absorbed dose is (Carlsson

1985, Berger et al. 2010):

$$D = \phi E \frac{\mu_{en}}{\rho} \tag{1}$$

with ϕ the particle fluence and $\frac{\mu_{en}}{\rho}$ the mass energy absorption coefficient.

The total track length $\mathrm{d}L$ of all particles crossing a given elementary volume $\mathrm{d}V$ around point $\boldsymbol{r}$ in the space (Carlsson 1985) gives us the fluence:

$$\phi(\boldsymbol{r}) = \frac{\mathrm{d}L(\boldsymbol{r})}{\mathrm{d}V} \tag{2}$$

Thus, for a given photon crossing a voxel with volume V, a good estimate of the contribution to the fluence will be given by (DeMarco et al. 2002, Williamson 1987):

$$\phi = \frac{L}{V} \tag{3}$$

with L being the length of the photon path within the given voxel. With such a method the dose is equal to:

$$D = \frac{EL\mu_{en}}{V\rho} \tag{4}$$

Unlike the MC analog estimator in which only the simulated collisions occurring within the voxel contribute to the dose, the use of the TLE will improve the efficiency of the simulation since every voxel intersected by a photon path will produce a non-zero dose score leading to a large increase of information that can be extracted from a finite sample of histories. For low energy photons, when considering the CPE, such a method uses the kerma approximation for which electrons are assumed to deposit their energy locally within a single voxel (thus, MC transport of secondary electrons can be switched off). Systematic deviations of the dose distributions can be minimized with this approach if the maximum range of secondary electrons is smaller than the spatial resolution of the calculation grid. That is why this approximation is valid only if the electron range is smaller than the voxel size or the required spatial accuracy (Seco & Verhaegen 2013).

For low energy photons, the linear energy-absorption (μ_{en}) and energy-transfer (μ_{tr}) coefficients can be considered to be the same quantity due to the fact that the radiative loss (factor g in Eq 5) approches zero for low values of atomic numbers and energy (Attix 2004, Berger et al. 2010, Freud et al. 2008):

$$\mu_{en} = \mu_{tr}(1 - g) \tag{5}$$

In human tissues, (made of elements with atomic numbers $Z \leq 20$), the relative difference between μ_{tr} and μ_{en} remains below 1% for energies up to 3 MeV and reaches a value of 3% for 10 MeV photons (Attix 2004).

1.1.2 Neutron dose calculation and CPE equilibrum validity

The photoneutron energies involved in radiotherapy ranges from thermal (0.025 eV) to fast (mean energy of 1 MeV). Since the human body consists of about 95% of hydrogen, carbon, oxygen and nitrogen (ICRU 2000),

the neutron dose will be deposited in the tissue through different processes. The elemental contribution to the kerma in soft tissues depends on neutron energy (Chadwick et al. 1999).

For a single neutron energy E, a single type of target atoms and a single type of interaction, the kerma K that results from a neutron fluence ϕ [n/cm^2] at a point in a medium is given by (Caswell et al. 1980):

$$K = \phi E \frac{\mu_{tr}}{\rho} = \phi \frac{N_t E_{tr} \sigma}{m} \tag{6}$$

where σ is the interaction cross section per target atoms, N_t is the number of target atom in the irradiated sample, m is the sample mass, and E_{tr} is the total kinetic energy given to charged particles per interaction. When considering the usual CPE conditions, the absorbed dose D is thus equal to the kerma K as:

$$D = K = \phi F_n \tag{7}$$

where F_n the kerma factor [cGy cm^2/n] is defined as

$$F_n = 1.602 \times 10^{-8} N_t E_{tr} \sigma / m \tag{8}$$

whith σ in [cm^2/(target atom)], m in [g] and E_{tr} in [MeV/n].

Tables of F_n values are found in the 46 ICRU report for energies between 0.025 eV to 20 MeV (Caswell et al. 1980) for several elements, compounds, and mixtures principally calculated from the ENDF/B-IV cross section library. The 63 ICRU report includes kerma coefficients determined from the latest ENDF/B-VI evaluated data libraries (Rose 1991) below 20 MeV and uses advanced nuclear model calculations and experimental information from 20 MeV to 150 MeV (the "LA150 data library" (Chadwick et al. 1999)). However, this update of kerma factors produced only a very small ($< 2\%$) difference in kerma calculations (Goorley et al. 2002) meaning that finally the use of either kerma databases is suitable

If we consider a continuous spectrum with a differential fluence distribution $\phi'(E)$ [n·cm^{-2}·MeV^{-1}], the kerma contribution by j-type interactions with i-type target atoms is (Attix 2004):

$$K_{ij} = 1.602 \times 10^{-8} \frac{N_i}{m} \int_0^{E_{max}} \phi'(E)\, \sigma_{ij}(E)\, [E_{tr}(E)]_{ij}\, \mathrm{d}E \tag{9}$$

with N_i/m the number of target atoms of type i per gram of the medium, $\sigma_{ij}(E)$ the cross section for j-type interactions with i-type atoms by neutrons of energy E, and $[E_{tr}(E)]_{ij}$ the total kinetic energy transferred to charged particles per type-j interactions with type-i atoms by neutrons of energy E.

For the same units as in Eq 6, K_{ij} [cGy] can be summed over all atoms i and all interactions j to get the kerma (or dose) due to all types of interactions and target atoms:

$$D = K = \sum_i \sum_j K_{ij} \tag{10}$$

When it comes to neutron interactions in tissue, we will have to consider thermal neutron reactions and fast

neutron reactions (Figure 1).

For the thermal neutrons reactions, there are two important interactions with tissues: neutron capture by nitrogen, ^{14}N(n,p)^{14}C, and neutron capture by hydrogen, ^{1}H(n,γ)^{2}H. The nitrogen interaction releases a kinetic energy of $E_{tr} = 0.62$ MeV that is shared by the proton (0.58 MeV) and the recoiling nucleus (0.04 MeV). Since the range of the secondary proton approximates 10 µm in tissue, CPE exists and $K = D$ even in very small tissue samples.

Thermal neutrons have a larger total probability of capture by hydrogen atoms than by nitrogen atoms in muscle even though $\sigma_H = 3.32 \times 10^{-25}$ cm^2/atom $< \sigma_N = 1.84 \times 10^{-24}$ cm^2/atom, because, there are 40 times more H atoms than N atoms in tissue. The γ-ray photon energy released in each neutron capture is 2.2 MeV. This of course will not directly contribute to the kerma, since the γ-rays must interact and transfer energy to charged particles to produce kerma. If we consider an irradiated tissue mass, small enough to allow the γ-rays to escape, the kerma due to thermal neutrons is only that resulting from the nitrogen (n,p) interactions. In larger masses of tissue the γ-rays are increasingly reabsorbed before escaping, thus contributing to the kerma. The human body has an intermediate size, but it is large enough so the ^{1}H(n,γ)^{2}H process dominates the kerma (and dose) production, not only for thermal neutrons but for intermediate energy neutrons as well, as they become themalised in the body.

For neutron energy above 10^{-4} MeV, elastic scattering from hydrogen nuclei contribute nearly all of the kerma.

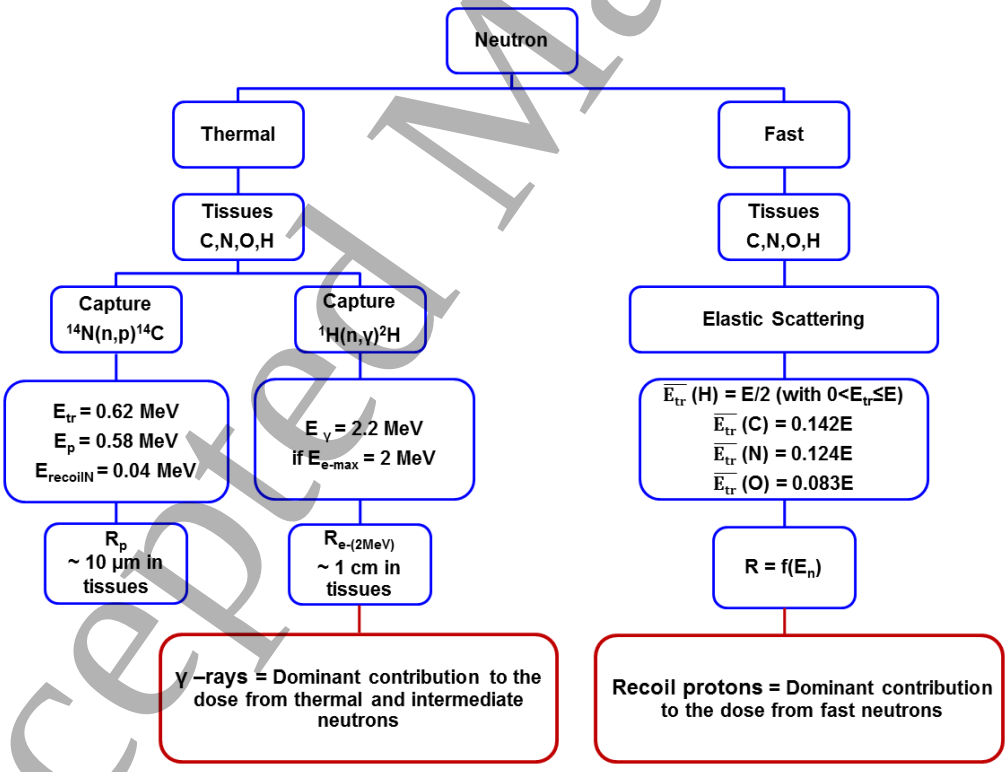

Figure 1: Main neutron interactions involved in soft tissue dose deposition

Given the energy range of the secondary neutrons produced in the radiotherapy accelerator head, for all dose components except the photon dose, the charged particles involved in the dose delivery to the tissues have ranges smaller than the general mesh element size (1 mm) of the dose scoring grid, leading to a good

approximation of the dose by the kerma. However, energetic electrons that can be produced through secondary photons interactions in tissue can have a range over 1 cm, similar to or larger than the dose grid element size. For example 2.2 MeV photons, mainly generated in soft tissues due to the capture of thermal neutron by Hydrogen nuclei, will induce the production of 2 MeV electrons (maximal Compton electron energy from the 2.2 MeV gamma). For the ICRP and cylindrical phantom simulation, the range of the 2 MeV generated electrons (maximal range of 1 cm and mean range of about 5 mm) can be larger than the spatial resolution of the phantom. The charged particle equilibrium hypothesis and the kerma approximation in each voxel could thus be not totally respected which can lead to a (small) dose overestimation in the voxel by the nTLE.

1.2 Implementation of Neutron TLE (nTLE) in GATE

1.2.1 Kerma factor

Similarly to the low energy photon, for a neutron crossing a volume V a good estimate of the dose is also given by Eq 7 ($\phi = L/V$) thus:

$$D = \frac{L}{V} F_n \tag{11}$$

To proceed with the neutron dose calculation, kerma factor tables have been generated for the different elements contained in the ICRU report 46 (Caswell et al. 1980). These factors are available for a large choice of human tissues, and within an energy interval ranging from 0.0253 eV to 29 MeV. For energies between 0.0253 eV and 29 MeV, as mentionned in (Chadwick et al. 1999), a linear interpolation has been used to obtain kerma coefficients at energies not tabulated.

The accuracy of the ICRU 46 (ICRU 1992) report kerma factors is estimated to be:

- Below 10 MeV: 1% for hydrogen and 5% for carbon, nitrogen and oxygen
- From 10 MeV to 30 MeV: 1 to 2 % for hydrogen and 10 to 25 % for carbon. For nitrogen and oxygen, uncertainties may be even higher at some energies.

An important issue in relation with these neutron kermas is the treatment of neutrons below 0.0253 eV since this is the lowest reported data point. Indeed, with a neutron capture cross section inversely proportionnal to the neutron kinetic energy (1/v law), the thermal neutron kerma values will increase in the same way as $E_n^{-0.5}$ (with E_n the neutron energy (Siebert & Schuhmacher 1995)), making the energy region below 0.0253 eV a significant contributor to kerma. Two methods are available in the literature for the evaluation of neutron kerma below 0.0253 eV. The first one is to proceed with a log-log extrapolation of the kerma data points below 1 eV down to an energy where there are very few neutrons, such as 10^{-4} eV (Goorley et al. 2002). The second one, which was used in this work, is to assign to the neutrons below 0.0253 eV the kerma values corresponding to the lowest tabulated energy point (the same way as the default treatment in MCNP) (Goorley et al. 2002).

1.2.2 Photon dose calculation

To accelerate their simulations, some studies on the secondary neutron dose in radiotherapy calculations (Kry et al. 2009, Martínez-Ovalle et al. 2012) have been carried out without considering the secondary photon dose resulting from the thermal neutron capture by hydrogen nuclei. Only the so-called "genuine neutron (absorbed) dose" (Valentin 2003) that does not include the contribution by photons released in the body by neutrons has been considered.

However, for accurate dosimetric studies, the gold standard is to be able to consider every dose component. To take into account the secondary photon dose in soft tissue mainly due to the 2.2 MeV photon from the $^{1}H(n,\gamma)^{2}H$ process, photon kerma factors in our algorithm are based on mass energy absorption coefficients (μ_{en}/ρ) data both from the NIST database and for the body parts for which these coefficients are not recorded, from the ICRU report 46, which are derived from Hubbell's elemental data (Hubbell 1982). It has been reported that the difference between these two kerma sets produced no significant differences in dose calculations: the differences in photon kerma rate dose profiles were less than the statistical uncertainty in the difference between the profiles, which was 0.2% (Goorley et al. 2002).

To proceed with these photon dose calculations, two methods have been tested: an analytical correction method and the TLE method.

1.2.2.1 Analytical correction

Analogous to the kerma factor F_n and based on the Attix publication (Attix 2004), we define the radiative kerma factor R_γ as the energy given to γ-rays per unit mass of tissue and per unit fluence. The R_γ factor of thermal neutrons can be obtained from an equation similar to Eq 9, but replacing E_{tr} by E_{γ_i} (which corresponds to the γ-ray photon energy released in each i neutron capture) such as:

$$R_\gamma = 1.602 \times 10^{-6} m^{-1} \sum_i \sigma_i N_{t_i} E_{\gamma_i} \tag{12}$$

where σ_i is the neutron capture cross section for the i atom [cm^2/(target atom)], N_{t_i} is the number of i target atoms in the irradiated sample, m is the sample mass [g], and E_{γ_i} is the γ-ray photon energy released in each neutron capture [MeV].

Given the body tissue composition and the differences in terms of neutron radiative capture cross section of the main target atoms contained in the body (Table 1), only the neutron cross section with H targets will be considered in the next steps of the analytical correction.

Element	γ_{prompt} [MeV]	$\sigma_{capture}$ [barn]	$\Sigma_{capture}$ [cm^{-1}]	Atoms per g of muscle [g^{-1}]
H	2.2	0.3326	2.13×10^{-2}	6.09×10^{22}
C	1.3	0.0012	7.77×10^{-6}	6.17×10^{21}
	4.9	0.00262	1.70×10^{-5}	
N	1.9	0.01458	2.31×10^{-5}	1.506×10^{21}
O	0.9	0.000175	5.13×10^{-6}	2.79×10^{22}

Table 1: Neutron capture cross section and prompt γ energies (International Atomic Energy Agency. 2007) in the case of skeletal muscle composition given by ICRU report 46 (ICRU 1992)

The R_γ factor of thermal neutrons will be thus obtained again from an equation similar to Eq 9, but replacing E_{tr} by $E_\gamma = 2.2$ MeV such as:

$$R_\gamma = 1.602 \times 10^{-6} \sigma N_t m^{-1} E_\gamma \tag{13}$$

where σ is the H interaction cross section [cm^2/(target atom)], N_t is the number of H atoms in the irradiated sample, m is the sample mass [g], and E_γ is the γ-ray photon energy released in each neutron capture [MeV]. From the simulation, the knowledge of the thermal neutron flux, as well as the knowledge of the quantity of H nuclei per gram of body material would thus allow a calculation of the contribution to the dose from the photons. A tabulation of this radiant energy per body material has been considered in this work in order to reduce the simulation time, since in such a configuration, the photons would not be longer tracked in the simulation. With such a method the deposited photon dose in a voxel of V volume will be equal to:

$$D_\gamma = R_\gamma \times \phi = R_\gamma \times \frac{L}{V} \tag{14}$$

1.2.2.2 TLE photon correction

The TLE method, as mentionned in 1.1.1, has been implemented in GATE for low energy photons. For the neutron dose calculation, the main contribution to the dose from photons is due to the 2.2 MeV photons from thermal neutron capture by hydrogen. The comparison between the μ_{en} and μ_{tr} (Attix 2004) for photon energies up to 3 MeV showed a difference between these two coefficients lower than 1% which comforts us in testing the performances of this TLE correction in our neutron dose calculation algorithm. The photon dose would thus be calculated as per Eq 4.

1.2.3 Total dose calculation

Finally, the total neutron dose D_{tot} deposited in a voxel, is calculated by the algorithms

- for the analytical correction such as:

$$D_{tot} = \sum_{k \in \mathrm{n}} (D_k + D_{\gamma,k}) = \frac{1}{V} \sum_{k \in \mathrm{n}} (F_{n,k} + R_{\gamma,k}) L_k \tag{15}$$

  with, for a given neutron k, the neutron dose D_k, the γ dose $D_{\gamma,k}$, the kerma factor $F_{n,k}$, the radiative factor $R_{\gamma,k}$, and the distance L_k travelled by the neutron k in a volume element V.

- for the TLE correction such as:

$$D_{tot} = \sum_{k \in \mathrm{n}} D_k + \sum_{l \in \gamma} D_{\gamma,l} = \frac{1}{V} \left(\sum_{k \in \mathrm{n}} F_{n,k} L_k + \sum_{l \in \gamma} E_l \frac{\mu_{en,l}}{\rho} L_l \right) \tag{16}$$

  with the neutron dose D_k of neutron k, the γ dose $D_{\gamma,l}$ of gamma l, L_k (resp. L_l) the distance travelled by the neutron k (resp. the gamma l) in a volume element V.

1.3 Simulation Test Cases

Different simulations have been performed in order to benchmark the nTLE algorithm against analog Monte Carlo simulations, in terms of dose calculation accuracy and variance reduction factor. Since the accuracy of the dose calculation by the algorithm had to be evaluated, a cut of 1 mm for γ and electrons was set: in each material, this value is transformed to an energy below which the continuous slowing down approximation is used. Furthermore, secondary particles below this energy are not produced, but the energy is deposited locally (Agostinelli et al. 2003). A cut of 0.1 mm was set for protons. To be able to fully compare the MC dose calculation and the nTLE dose calculation as well as the gain in terms of variance, simulations with an identical seed have been carried out.

Simulations have been carried out first in homogeneous cubic volumes to fully validate the dose calculation before proceeding with simulations on a heterogeneous phantom and voxelized phantom. Regarding the voxelisation of the volumes (simple volume or phantom), it is relevant to mention that since MC generation can use any resolution, both isotropic and anisotropic voxel size can be used by the method without any advantage given to one or other of voxel type. While any resolution can be used with the nTLE (using for example XCAT phantom (Segars et al. 2010)), the main concern would not be the shape of the voxel (isotropic or anisotropic) but its volume.

Moreover, since in high energy X-ray treatments we get mainly thermal neutrons (around 0.025 eV) and a fast neutron component (around 1 MeV), monoenegetic neutron beams of 0.025 eV and 1 MeV have been simulated to study the impact of the neutron energy on the dose calculation accuracy and on the variance reduction factor. The energy of 10 MeV has also been simulated to evaluate the performances of the algorithm at higher energies.

1.3.1 Simple homogeneous volume

The first step was to proceed with a benchmarking of the photon dose correction impact on the neutron dose calculation. Since the human body is mainly composed of soft tissues, the simulations were first carried out on simple cubic geometry configurations of muscle tissue. This allowed us to fully measure the algorithm's performance with the different photon dose corrections and its ability to give an accurate neutron dose calculation in comparison with the analog MC method. To do so, simulations were first carried out on cubes consisting of ICRU 44 skeletal muscle of various sizes with a density of 1.05 g·cm^{-3}. The composition is given as per the ICRU report 46 composition in Table 2.

Element	H	C	N	O	Na	P	S	Cl	K
Percent by weight [%]	10.2	14.3	3.4	71.0	0.1	0.2	0.3	0.1	0.4

Table 2: Skeletal muscle composition given by ICRU report 46 (ICRU 1992)

Monoenergetic neutron sources (10^6 particles) with energies relevant in radiotherapy irradiated soft tissue targets. The tested energies were 0.025 eV, 0.1 MeV, 1 MeV and 10 MeV.

1.3.2 Voxelised cases

1.3.2.1 Heterogeneous volume

Simulations with monoenergetic neutron beams impinging upon a simple voxelised volume were used to evaluate the nTLE performances of dose calculation accuracy and variance reduction. Given the fact that mean voxel resolution is of the order of a few mm^3 in the computational phantom models, simulations on a voxelised (1 mm^3 voxels) cylindrical soft tissue volume (diameter of 33 cm) were made. Eight inserts (diameter of 3 cm) of Griffith lung tissue 0.26 $g{\cdot}cm^{-3}$ (ICRU 1992), and eight inserts of cortical bone, 1.920 $g.cm^{-3}$ (ICRU 1992), were added to test the performances of the nTLE algorithm in terms of the dose calculation in an heterogeneous volume. Monoenergetic planar neutron sources of 0.025 eV, 1 MeV and 10 MeV irradiated the cylindrical volume. To ensure an homogeneous irradiation of the volume, the cylinder was rotated around its long axe.

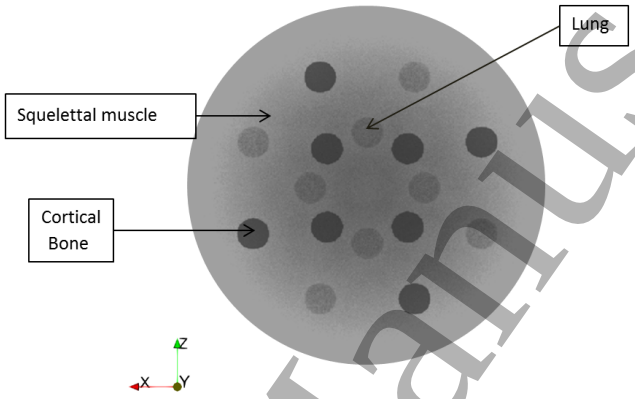

Figure 2: Transverse section of the cylindrical geometry with its heterogeneities

1.3.2.2 ICRP phantom

In order to assess the potential of the nTLE method to produce dose distributions in realistic cases and to evaluate the gain in variance reduction, two simulations were performed using a voxelized ICRP phantom (publication 110) (ICRP 2009) as input to define the geometry and composition of the volume in which the dose deposition would be evaluated (Figure 3). The voxel size was 2.1 mm × 2.1 mm × 8 mm for a total voxel volume of about 35.3 mm^3. A typical neutron spectrum measured in a treatment room (Chu et al. 2011) irradiated the pelvis area of the phantom. The object was rotated around an axis perpendicular to the beam direction in order to produce a homogeneous irradiation. About 3×10^{10} particles were incident on the phantom in order to have a statistical uncertainty lower than 1% with the analog MC dose calculation to accurately assess our algorithm dose calculation performances.

1.3.2.3 Comparison parameters for benchmarking against analog MC

Dose ratio To check the dose calculation accuracy of the nTLE against the MC method, dose ratio maps ($r_{Analog/nTLE}$) have been generated such as:

$$r_{Analog/nTLE} = \frac{D_{Analog}}{D_{nTLE}} \tag{17}$$

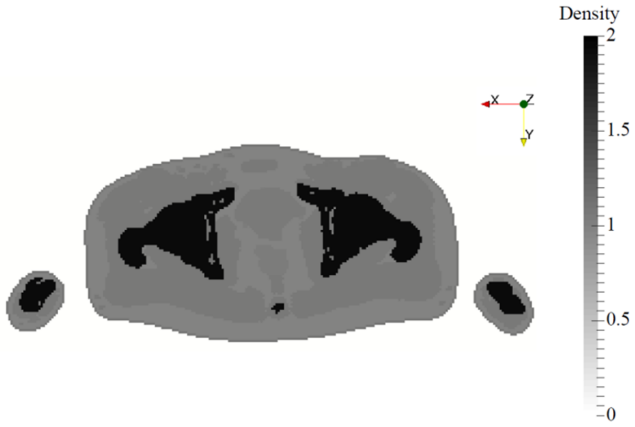

Figure 3: ICRP phantom slice densities

Statistical uncertainty To measure the differences in regards to the statistical uncertainties for the same simulation parameters, dose maps representing the uncertainty ratios ($r_{Analog/nTLE}$) at the three simulated energies have been generated such as:

$$r_{Analog/nTLE} = \frac{\sigma_{Analog}}{\sigma_{nTLE}} \tag{18}$$

with σ_{Analog} the statistical uncertainty of the analog MC dose calculation and σ_{nTLE} the statistical uncertainty of the nTLE algorithm.

Then, the estimation of the number of events N_t required to get a statistical error of about σ_t is (Mittone et al. 2013):

$$N_t = \left(\frac{\sigma_i}{\sigma_t}\right)^2 N_i \tag{19}$$

with σ_i and σ_t the standard deviations, N_i and N_t number of simulated events.

The ratio N_t/N_i can be easily related to the gain in computing time. However these values have to be corrected considering the fact that the nTLE algorithm requires about 10% more computation time in comparison to the MC with the same simulation seed. These ratios are given by Figures 6 and 8.

2 Results

2.1 Simple homogeneous volume

Figure 4 presents the differences of dose calculation by the different methods. The stars, squares, circles and triangles respectively represent the dose calculated with the analog MC method, algorithm without photon correction, algorithm with analytical photon correction (1.2.2.1) and with TLE photon correction (1.2.2.2). It clearly appears from these figures, that the photon dose calculation has to be taken into account in order to not underestimate the neutron deposited dose, while on the other hand the TLE photon correction allows a better photon dose calculation. Indeed for almost all the configurations, maximal dose calculational differences are lower than 3% compared to the MC calculation except for the 1 mm^3 case with incident neutrons of 10 MeV where we get a 40% dose overestimation by the algorithm. This overestimation is due to the fact that with 10 MeV neutrons, protons up to 10 MeV will be produced: these protons have a range of around 1 mm in the soft tissues which produces an unsatisfied CPE condition which in turn leads to a dose overestimation by the

algorithm. For the other tested volume sizes, since CPE is fullfilled, this overestimation no longers occurs with the TLE photon correction.

At thermal neutron energy, the analytical correction shows two divergences compared to the MC method. It shows an overestimation of the dose when used in both the 1 mm^3 and 1 cm^3 volumes for the thermal neutron energy. This overestimation is due to the fact that with this correction, neutrons with energies lower than or equal to 0.025 eV are considered to be systematically captured by the H nuclei of the target, leading to a systematical local dose deposition from the generated 2.2 MeV photons as per Eq 15. When a larger volume is considered, the analytical correction leads to an underestimation of the dose (30%). The analysis of the generated photon spectrum inside the target excluding the capture generated photons showed that this difference is due to other photons interactions processes that are not taken into account by the analytical correction such as bremsstrahlung effects, pair creation and Compton scattered photons.

Given these observations, the TLE photon correction has been chosen over the analytical correction for the rest of our work.

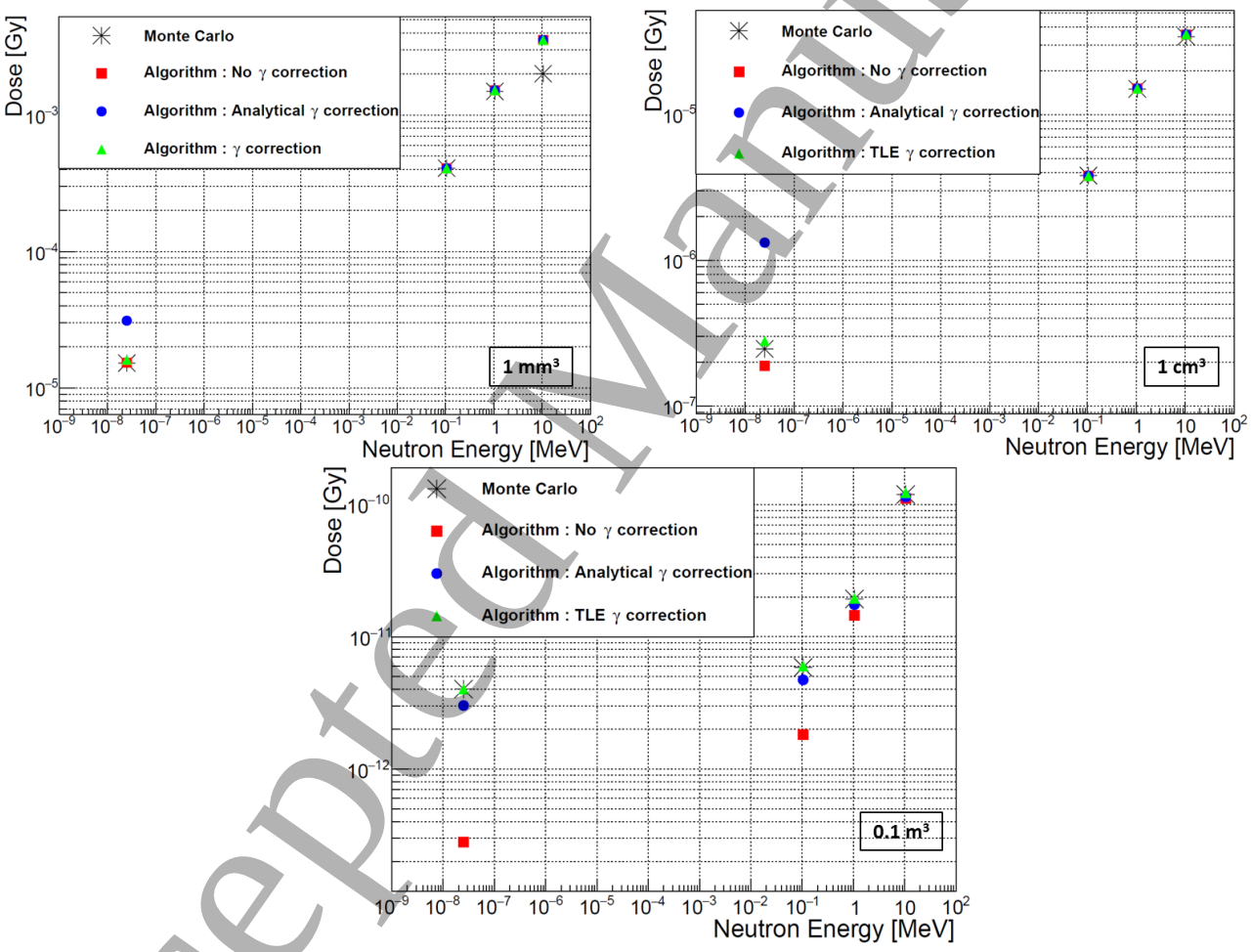

Figure 4: Comparison of dose calculation by the nTLE algorithm with the different photon dose corrections vs the MC dose calculation in different skeletal muscle cubical volumes

2.2 Voxelised heterogeneous volume case

2.2.1 Dose calculation

The dose ratio for the different simulated neutron energies are represented in Figure 5. At thermal energies, the mean dose differences between the nTLE and the analog MC over the whole volume is about 3%. However the dose difference can reach a maximum of 25% for a few voxels especially in the lung area. For the 1 MeV irradiation, the mean difference is about 1% except in the central lung inserts. For the 10 MeV neutron energy, the mean difference is lower than 1% in the whole volume except at the boundaries of the different materials. These differences are linked to the range of the secondary charged particles responsible for the dose deposition, the voxel size and the local dose approximation made by the nTLE algorithm.

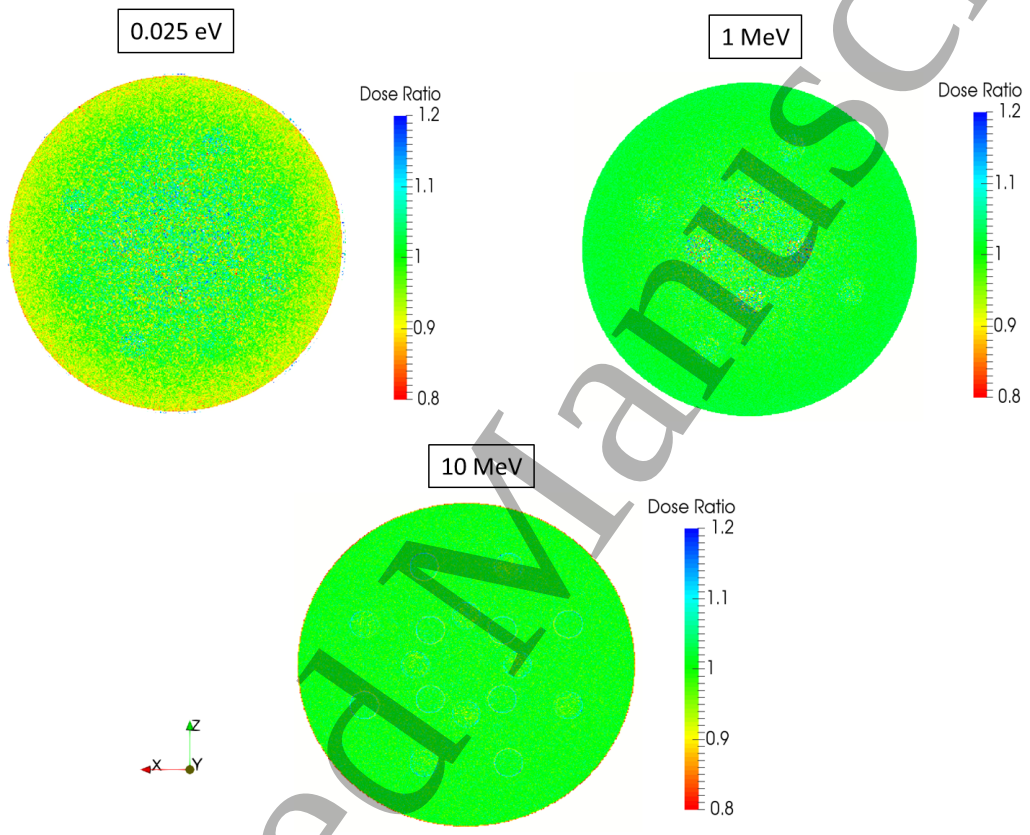

Figure 5: Dose ratio (analog over nTLE) for the different simulated neutron energies.

2.2.2 Statistical uncertainty

The uncertainty ratios for the different simulated neutron energies are represented in Figure 6. These ratios show that a factor of 4 to 20 can be obtained depending on the energies of the incident particles and the materials. The nTLE dose algorithm allows thus an increase of the calculation speed up to 400 times compared to the *DoseActor* of GATE. To be able to fully evaluate the gain in the phantom, an uncertainty ratio profile (Figure 7) has been plotted for each energy across a line in the middle of the slice crossing two lung inserts. It appears clearly that the speed gain is affected both by neutron energy and medium composition.

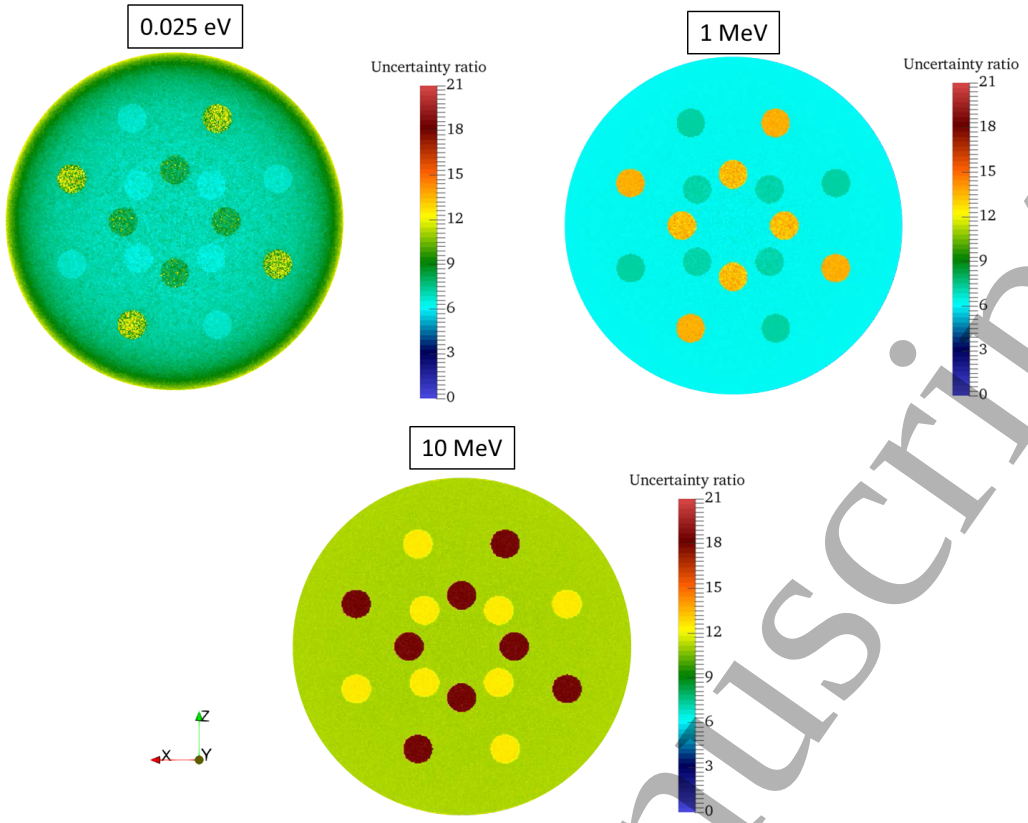

Figure 6: Uncertainty ratios (analog over nTLE) for the different simulated neutron energies.

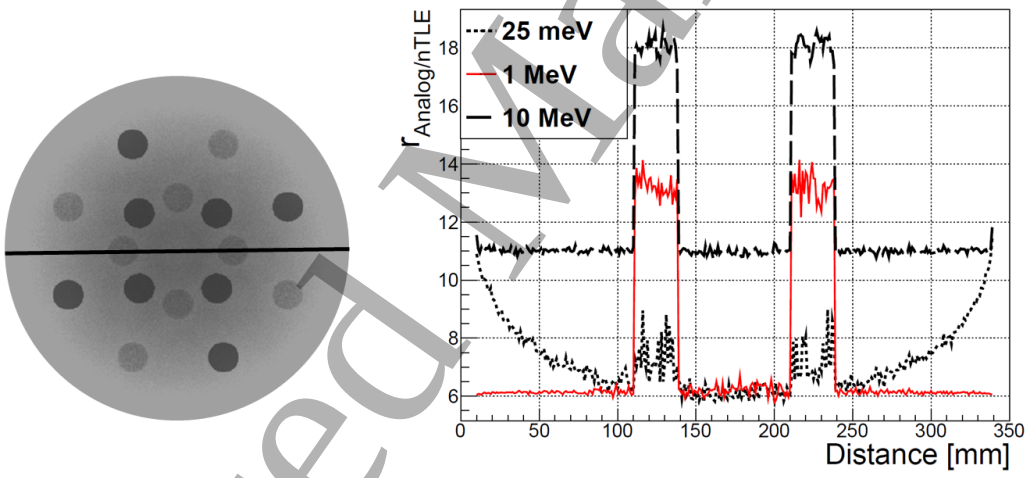

Figure 7: Uncertainty ratio profiles (analog over nTLE) for the different simulated neutron energies along the black line.

2.3 Voxelised ICRP phantom

2.3.1 Dose calculation

The left side of Figure 8 represents the dose ratio map. The mean dose ratio between the analog MC and the nTLE of the slice is 0.998 (0.992 in the central area). These results show a very good agreement of the nTLE algorithm with the MC method for dose calculation in a realistic radiotherapy case.

2.3.2 Statistical uncertainty

Results in terms of statistical uncertainty ratios are shown on Figure 8. For a realistic neutron spectrum in a radiotherapy room (mean energy around 1 MeV) and a voxel volume of 35.3 mm^3 the mean simulation time

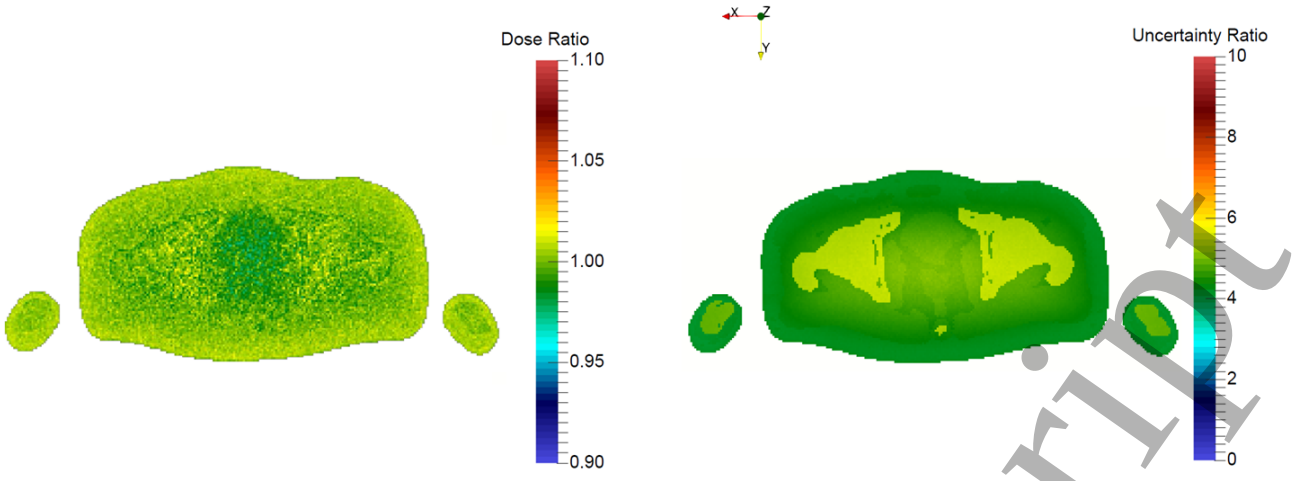

Figure 8: Left: Dose ratio (analog over nTLE) ; Right: Uncertainty ratio (analog over nTLE) for the pelvis of a voxelised ICRP phantom irradiated with a realistic neutron spectrum.

gets accelerated by a factor from about 15 to 40 depending mainly on tissue compositions. This factor appears to be much lower than the one found with the heterogeneous phantom (voxel size = 1 mm^3) at the energy of 1 MeV. This is due to the fact that the acceleration factor is inversely proportional to the voxel size.

3 Discussion

The main goal of this work was to develop an efficient tool for neutron dose calculation in radiotherapy. The results of cylindrical phantom with the monoergetic neutron beams allowed us to evaluate the performances of our algorithm and the origin of possible inaccuracies on dose calculation. When considering the thermal neutron beam with a voxelisation of 1 mm^3, the comparison of the nTLE dose calculation to the MC method showed an average difference of 7% in the peripheral area of the phantom. This difference is due to the local dose approximation made in the nTLE method. At the thermal energy, neutrons captured by the H nuclei will generate photons of 2.2 MeV that will lead to the production of secondary electrons with energies up to 2 MeV. The range of these electrons is 1 cm in soft tissue and 4 cm in the lung. In a 1 mm^3 voxelised volume, in the first layers of the volume the generated electrons are too energetic to deposit their dose localy in the voxel which leads to an overestimation of the dose by the nTLE in the concerned voxel, the charged particle equilibrum not beeing fulfilled. However, deeper in the phantom layers (central area of the phantom), charged particle equilibrum becomes etablished which leads to a better dose calculation by the algorithm, with a mean difference close to 1% with the analog MC. For energies of 1 MeV, this peripheral dose overestimation does not appear, since at these energies, the energy is mainly deposited through scattered protons which have a range in tissue of less than 1 mm. However, once these neutrons get thermalised and captured by H, photons and electrons will be generated which explains the overestimation of the dose in the lung tissue in the middle of the phantom, due to the range of the secondary electrons in such a tissue. At this energy the mean difference in the dose calculation between the dose actor and the nTLE is estimated to be about 1% except for the pulmonary region, where the non fulfillment of the CPE condition leads to a maximal difference of 20% in comparison with the analog MC. When we evaluate the performances of the nTLE at a higher energy such as 10 MeV, the dose ratio map shows an accuracy with a mean dose difference of 1% with the analog MC except at the voxel

delimiting the interface of two different materials.

When a typical neutron energy spectrum in radiotherapy irradiated the pelvis region of an ICRP phantom, the mean discrepancy between the analog MC and the nTLE is less than 1% (mean dose ratio of 0.998 over the slice). This is explained on one hand by the fact that in a radiotherapy treatment the main component of the spectrum are neutrons with a mean energy of 1 MeV while on the other hand, the ICRP phantom voxel size is 40 times bigger than the cylindrical phantom voxel size. In such a case the local dose deposition approximation made by the algorithm will be more valid and fulfilled. These results highlight both the fact that the nTLE allows us to have a good performance in terms of neutron dose calculation and the fact that it is feasible to use it in radiotherapy applications.

Regarding the variance reduction factor, it appears that it is mainly affected by the neutron energy, the material composition and the voxel size of the phantom. For neutron beams of 25 meV, 1 MeV and 10 MeV, the mean gain of computing time in muscle tissue is respectively about 60, 30 and 120 with voxels of 1 mm^3. At 1 MeV, with a similar voxel size, depending on the considered material, the mean gain of computing time is respectively about 200, 30 and 50 for the lung muscle and bone material. For a given voxel size, the cylindrical phantom simulation case allowed us to determine the fact that the gain will be increased by two factors: the mean free path of the particles and the density of the medium. Indeed, the longer the mean free path of the particle, the greater will be the gain, since with the nTLE approach we consider a continuous energy deposition in all the voxels crossed by the particle. The density of the medium will also have an impact on the gain as shown in Figures 6 and 7, where it clearly appears that the gain is in each case higher in the lung tissue due to its lower density in comparison with the bone and squelettal muscle. The change in the voxel size which is illustrated by the dose calculation in the pelvis of the phantom, shows a mean drop in the gain by a factor of 3, which indicates that the variance reduction factor will be higher when fine spatial resolutions are considered. Thanks to the nTLE, the mean gain obtained for dose calculations in the voxelised ICRP phantom is 25 times greater than the analog MC.

4 Conclusion

The neutron TLE algorithm (nTLE) developped in GATE has proven to be a precise and efficient tool for neutron dose calculation in radiotherapy. By reducing the mean calculation time by a factor 25 for a typical radiotherapy neutron spectrum on a computational phantom, the nTLE could be part of a future MC peripheral dose computation framework, dealing with neutron dose calculation, in order to systematically and accurately evaluate the neutron component generated through the different treatment parameters. The comprehensive study of its performances will allow its optimal use, especially when it comes to making the right compromise between the voxel size and acceleration factor. Thanks to this tool, the out-of-field neutron dose absorbed by the radiosensitive organs of a patient will be much easier to track and evaluate. While the present paper has focussed on high energy X-ray radiotherapy, the method developped could be used for other radiotherapy treatment involving neutrons (protontherapy, neutron capture therapy, hadrontherapy) when the sampling of the geometry does not compromise the CPE and local dose deposition approximations.

References

Agostinelli S et al. 2003 Geant4—a simulation toolkit *Nuclear Instruments and Methods in Physics Research Section A: Accelerators, Spectrometers, Detectors and Associated Equipment* **506**(3), 250–303.

Akkurt I et al. 2003 Photoneutron yields from tungsten in the energy range of the giant dipole resonance. *Physics in Medicine and Biology* **48**(20), 3345–52.

Athar B S et al. 2010 Comparison of out-of-field photon doses in 6 MV IMRT and neutron doses in proton therapy for adult and pediatric patients. *Physics in Medicine and Biology* **55**(10), 2879–91.

Attix F H 2004 Introduction to Radiological Physics and Radiation Dosimetry p. 505.

Battistoni G et al. 2007 The FLUKA code: Description and benchmarking *in* 'AIP Conference Proceedings' Vol. 896 pp. 31–49.

Berger M J et al. 2010 XCOM: Photon Cross Sections Database *NIST Standard Reference Database 8 (XGAM)* .

Brenner D J et al. 2000 Second malignancies in prostate carcinoma patients after radiotherapy compared with surgery. *Cancer* **88**(2), 398–406.

Carinou E et al. 2005 An MCNP-based model for the evaluation of the photoneutron dose in high energy medical electron accelerators *Physica Medica* **21**(3), 95–99.

Carlsson G A 1985 *in* 'Theoretical Basis for Dosimetry, Chap. 1 in The Dosimetry of Ionizing Radiation, Vol. 1, K.R. Kase, B.E. Bäjrngard and F.H. Attix, eds.' pp. 1–75.

Caswell R S, Coyne J & Randolph M 1980 Kerma factors for neutron energies below 30 MeV *Radiation Research* **83**(2), 217–254.

Chadwick M et al. 1999 Cross-section evaluations to 150 MeV for accelerator-driven systems and implementation in mcnpx *Nuclear Science and Engineering* **131**(3), 293–328.

Chen C et al. 2006 A detailed study on the neutron contamination for a 10MeV medical electron accelerator *Nuclear Instruments and Methods in Physics Research Section A: Accelerators, Spectrometers, Detectors and Associated Equipment* **562**(2), 1033–1037.

Chibani O et al. 2005 MCPI (c): A sub-minute Monte Carlo dose calculation engine for prostate implants. *Medical Physics* **32**(12), 3688–3698.

Chu W et al. 2011 Neutron spectrometry and dosimetry around 15 MV linac *Radiation Measurements* **46**(12), 1741–1744.

DeMarco J J et al. 2002 A Monte Carlo tutorial and the application for radiotherapy treatment planning *Medical Dosimetry* **27**(1), 43–50.

D'Errico F et al. 1998 In-phantom dosimetry and spectrometry of photoneutrons from an 18 MV linear accelerator. *Medical Physics* **25**(9), 1717–24.

Ferrari A et al. 2005 Fluka: a multi-particle transport code *in* 'CERN 2005-10 (2005), INFN/TC 05/11, SLAC-R-773'.

Freud N et al. 2008 A hybrid approach for fast simulation of dose deposition in stereotactic synchrotron radiotherapy *in* 'IEEE Transactions on Nuclear Science' Vol. 55 pp. 1008–1017.

Goorley J T et al. 2002 Reference dosimetry calculations for neutron capture therapy with comparison of analytical and voxel models. *Medical Physics* **29**(2), 145–156.

Gudowska I et al. 2014 Radiation burden from secondary doses to patients undergoing radiation therapy with photons and light ions and radiation doses from imaging modalities *Radiation Protection Dosimetry* **161**(1-4), 357–362.

Halg R A et al. 2012 Systematic measurements of whole-body dose distributions for various treatment machines and delivery techniques in radiation therapy. *Medical Physics* **39**(12), 7662–76.

Howell R et al. 2006 Calculation of effective dose from measurements of secondary neutron spectra and scattered photon dose from dynamic MLC IMRT for 6 MV, 15 MV, and 18 MV beam energies. *Medical Physics* **33**(2), 360–8.

Huang W et al. 2005 Calculation of photoneutrons produced in the targets of electron linear accelerators for radiography and radiotherapy applications *Nuclear Instruments and Methods in Physics Research Section B: Beam Interactions with Materials and Atoms* **229**(3), 339–347.

Hubbell J 1982 Photon mass attenuation and energy-absorption coefficients *The International Journal of Applied Radiation and Isotopes* **33**(11), 1269–1290.

Huisman B F B, Létang J M, Testa É & Sarrut D 2016 Accelerated prompt gamma estimation for clinical proton therapy simulations *Physics in Medicine and Biology* **61**(21), 7725–7743.

ICRP 2007 Preface, Executive Summary and Glossary *Annals of the ICRP* **37**(2-4), 9–34.

ICRP 2009 Adult Reference Computational Phantoms. ICRP Publication 110. Technical Report 2.

ICRU 1992 Neutron interaction data for body tissues *ICRU Report* **46**, 1–8.

ICRU 2000 Nuclear Data for Neutron and Proton Radiotherapy and for Radiation Protection (Report 63) Technical report.

International Atomic Energy Agency. 2007 *Database of prompt gamma rays from slow neutron capture for elemental analysis*. International Atomic Energy Agency.

Jan S et al. 2004 Gate: a simulation toolkit for pet and spect *Physics in Medicine and Biology* **49**(19), 4543.

Jan S et al. 2011 GATE V6: a major enhancement of the GATE simulation platform enabling modelling of CT and radiotherapy *Physics in Medicine and Biology* **56**(4), 881–901.

Jarlskog C Z et al. 2008 Sensitivity of different dose scoring methods on organ-specific neutron dose calculations in proton therapy. *Physics in medicine and biology* **53**(17), 4523–32.

Kawrakow I et al. 2000 Investigation of variance reduction techniques for Monte Carlo photon dose calculation using XVMC. *Physics in Medicine and Biology* **45**(8), 2163–83.

Kry S F et al. 2009 Neutron spectra and dose equivalents calculated in tissue for high-energy radiation therapy *Medical Physics* **36**(4), 1244–1250.

Luceski A et al. 2013 Validation of the GATE Monte Carlo code for radiation therapy and application to inhomogeneities *Physica Medica* **29**, e23.

Martínez-Ovalle S et al. 2012 Neutron dosimetry in organs of an adult human phantom using linacs with multileaf collimator in radiotherapy treatments *Medical Physics* **39**(5), 2854–2866.

Mesbahi A et al. 2009 A Monte Carlo study on neutron and electron contamination of an unflattened 18-MV photon beam. *Applied Radiation and Isotopes : including data, instrumentation and methods for use in agriculture, industry and medicine* **67**(1), 55–60.

Mittone A et al. 2013 An efficient numerical tool for dose deposition prediction applied to synchrotron medical imaging and radiation therapy *Journal of Synchrotron Radiation* **20**(5), 785–792.

Murray L et al. 2014 Second primary cancers after radiation for prostate cancer: A systematic review of the clinical data and impact of treatment technique *Radiotherapy and Oncology* **110**(2), 213–228.

Naseri A et al. 2010 A review on photoneutrons characteristics in radiation therapy with high-energy photon beams. *Reports of practical oncology and radiotherapy : journal of Greatpoland Cancer Center in Poznan and Polish Society of Radiation Oncology* **15**(5), 138–44.

Newhauser W D et al. 2011 Assessing the risk of second malignancies after modern radiotherapy. *Nature reviews. Cancer* **11**(6), 438–48.

Nievaart V A et al. 2007 *Spectral tailoring for boron neutron capture therapy* IOS Press.

Palm A et al. 2010 Absorbed dose and dose rate using the Varian OBI 1.3 and 1.4 CBCT system. *Journal of applied clinical medical physics* **11**(1), 3085.

Pelowitz D B 2008 MCNPX User'S Manual Version 2.6.0 *Los Alamos National Laboratory* .

Perl J et al. 2012 TOPAS: an innovative proton Monte Carlo platform for research and clinical applications. *Medical physics* **39**(11), 6818–37.

Poludniowski G et al. 2009 An efficient Monte Carlo-based algorithm for scatter correction in keV cone-beam CT *Physics in Medicine and Biology* **54**(12), 3847–3864.

Reft C S et al. 2006 In vivo and phantom measurements of the secondary photon and neutron doses for prostate patients undergoing 18 MV IMRT. *Medical physics* **33**(10), 3734–42.

Rose P 1991 ENDF-201: ENDF/B-VI summary documentation Technical report Brookhaven National Lab., Upton, NY (United States).

Sarrut D et al. 2014 A review of the use and potential of the GATE Monte Carlo simulation code for radiation therapy and dosimetry applications *Medical Physics* **41**(6), 064301.

Seco J & Verhaegen F 2013 *Monte Carlo Techniques in Radiation Therapy.*

Segars W P et al. 2010 4D XCAT phantom for multimodality imaging research *Medical Physics* **37**(9), 4902–4915.

Shultis J K et al. 2006 An MCNP Primer *Structure* **66506**(c), 0–45.

Siebert B & Schuhmacher H 1995 Quality Factors, Ambient and Personal Dose Equivalent for Neutrons, Based on the New ICRU Stopping Power Data for Protons and Alpha Particles *Radiation Protection Dosimetry* **58**(3), 177–183.

Smans K et al. 2010 Simulation of image detectors in radiology for determination of scatter-to-primary ratios using Monte Carlo radiation transport code MCNP/MCNPX *Medical Physics* **37**(5), 2082.

Smekens F et al. 2009 Simulation of dose deposition in stereotactic synchrotron radiation therapy: a fast approach combining Monte Carlo and deterministic algorithms. *Physics in medicine and biology* **54**(15), 4671–4685.

Smekens F et al. 2014 Split exponential track length estimator for Monte-Carlo simulations of small-animal radiation therapy. *Physics in medicine and biology* **59**(24), 7703–7715.

Takam R et al. 2011 Out-of-field neutron and leakage photon exposures and the associated risk of second cancers in high-energy photon radiotherapy: current status. *Radiation research* **176**(4), 508–20.

Taylor R E P et al. 2007 Benchmarking brachydose: Voxel based EGSnrc Monte Carlo calculations of TG-43 dosimetry parameters. *Medical physics* **34**(2), 445–457.

Valentin J 2003 Relative biological effectiveness (rbe), quality factor (q), and radiation weighting factor (w r): Icrp publication 92 *Annals of the ICRP* **33**(4), 1–121.

Van der Zee W et al. 2005 ORANGE: a Monte Carlo dose engine for radiotherapy *Physics in Medicine and Biology* **50**(4), 625–641.

Walters B R B et al. 2002 History by history statistical estimators in the BEAM code system *Medical Physics* **29**(12), 2745–2752.

Williamson J F 1987 Monte Carlo evaluation of kerma at a point for photon transport problems. *Medical physics* **14**(4), 567–76.

554 Xu X G et al. 2008 A review of dosimetry studies on external-beam radiation treatment with respect to second
555 cancer induction. *Physics in medicine and biology* **53**(13), R193—-241.